Copyright
by
Katherine Elizabeth Olin
2018

The Thesis committee for Katherine Elizabeth Olin
certifies that this is the approved version of the following thesis:

Characterizing the depth dependence of resolution and signal strength for two-photon microscopy

APPROVED BY

SUPERVISING COMMITTEE:

Andrew K. Dunn, Supervisor

James Tunnell

Characterizing the depth dependence of resolution and signal strength for two-photon microscopy

by

Katherine Elizabeth Olin

THESIS

Presented to the Faculty of the Graduate School of

The University of Texas at Austin

in Partial Fulfillment

of the Requirements

for the Degree of

MASTER OF SCIENCE IN ENGINEERING

THE UNIVERSITY OF TEXAS AT AUSTIN

May 2018

To my mother and father.

Acknowledgments

I would like to thank Andrew Dunn for providing vital feedback to my experimental attempts. I also would like to thank my lab members for their contributions to my experiments and my overall knowledge. I could not have completed my work without David Miller, Jeremy Jarrett, Colin Sullender, and especially Ahmed Hassan.

Characterizing the depth dependence of resolution and signal strength for two-photon microscopy

Katherine Elizabeth Olin, M.S.E.
The University of Texas at Austin, 2018

Supervisor: Andrew K. Dunn

Two-photon (2P) microscopy is a useful tool for studying structure and function of biological samples. As optical optimizations occur in 2P systems that allow imaging at deeper depths, there is a need to characterize the resolution and the signal interactions with tissue at these depths. Here, we discuss processes to determine the resolution of a 2P microscope using sub-resolution sized micro-spheres to mimic point spread functions. Through this process, the resolution of the microscope was determined to be about 0.942 µm *in vitro* and about 1.08 µm *in vivo*, values that did not change with respect to depth. Additionally, we investigated the relationship between contrast, background intensity, and noise with depth *in vivo*. From this study, contrast decreased with depth, while background intensity and noise both increased. These results suggest that the decrease in resolving power at deep depths is likely due to the inability to differentiate signal from background and not due to a decrease in the overall resolution of the system.

Table of Contents

List of Tables

List of Figures

Chapter 1

Introduction

1.1 Two-Photon Microscopy

Fluorescent imaging has allowed researchers to examine biological structure and function. Relying on the process of fluorescence, fluorescent imaging uses high-energy excitation light to generate low-energy emission light from a sample. Fluorescence occurs when a fluorophore absorbs a photon of light and is excited to a high energy state. Upon relaxation to its initial energy state, the fluorophore emits a photon that can be detected. When many of these photons are emitted, an image of the glowing items can be produced.

All fluorescent imaging *in vivo* requires fluorescent agents to be either injected into or attached onto biological materials. Because the imaging relies on a unique interaction between fluorophore type and wavelength of light, separate entities can be isolated by using different fluorophore types or distinct excitation wavelengths and depicted simultaneously in the same image. Such can be seen with vasculature and neurons in brain tissue depicted simultaneously [25]. The ability to isolate items of interest makes fluorescent microscopy a powerful tool in the crowded environment of biological samples.

One particular issue with traditional wide-field fluorescent imaging arises

when a large number of excitation photons bombard the sample. Because fluorophore throughout the sample can also be excited, incident light reaching the detector may not be limited to a definite focal spot. Laser scanning techniques, such as confocal microscopy and later two-photon (2P) microscopy, address this issue by introducing scanning optics and additional methods to reduce the detected fluorescence to within a specific focal volume. In particular, 2P microscopy works via simultaneous excitation of the fluorophore with two lower-energy photons: fluorophores with a 400-500 nm excitation wavelength can be excited with a light source of similar wavelength for traditional fluorescence or with an NIR light source using 2P microscopy. Because 2P excitation is a rare phenomenon under normal light intensities, mode-locked lasers that produce short pulses (˜100 fs) of high intensity coherent light are used to generate sufficient fluorescent signal. By focusing the short pulses into a sample, large numbers of photons are localized temporally at the focal volume while fewer photons are present outside the focus, reducing the amount of out-of-focus signal [14].

Using photons of lower energy, and thus increased wavelength, means 2P is more ideal than other fluorescent imaging techniques for imaging at deeper depths, since longer wavelengths of light penetrate further into biological tissue [20]. Recently, 2P microscopy has been used to generate images *in vivo* of depths up to or over 1 mm in mouse brain tissue, with depth limits that vary based on laser type [14, 17, 18, 30].

1.2 Resolution

Resolution is described as the minimal distance needed to distinguish two items from one another. The value is related to the point spread function (PSF), which describes how signal propagates from a point source. Images are formed as the convolution of an object's intensity profile with the PSF, meaning that when two objects are within a PSF's full width at half its maximum value (FWHM) of each other, they cannot be resolved [23].

Resolution is related to the wavelength of light and to the diffraction of light traveling through the imaging system. Diffraction in the optical system limits the lateral resolution to

$$\Delta_{x,y} \approx \frac{\lambda}{2 \cdot NA} \tag{1.1}$$

where λ is the wavelength and NA is the numerical aperture of the objective [3]. While the theoretical resolution equation provides an estimation of resolution, the absolute resolution can be determined by measuring the PSF seen in an image. For most images, however, separating the PSF from the object is challenging. Without precise knowledge of the object's shape, the object cannot be deconvolved from the image. To get around this difficulty, an object that approximates a point source can be used. Because a single point represents a delta function in space, objects smaller than the theoretical resolution can be used to isolate the PSF.

In a non-turbid medium, resolution is not expected to change with respect to depth [10]. Though in a scattering sample, photons outside the focal

point can reach the detector. In traditional fluorescent microscopy, this causes a decrease in resolution with increased depth, as more scattering events occur [10]. By solely exciting fluorophore within the focal volume, 2P microscopy ensures only photons originating from the focus are seen by the detector [14]. This suggests that the as long as sufficient signal is present, resolution of 2P microscopy is not influenced by image depth. Previous work has suggested that the PSF does not significantly change in surface-level depths of turbid *in vitro* samples [9]. However, depths similar to those in deep imaging and in *in vivo* samples have not been presented.

The goal of this research is to characterize the 2P microscopy resolution *in vivo*. Without full understanding of how signal and resolution behave throughout the sample, conclusions about objects near the resolution limit cannot be considered valid. The identity of such small objects may be suspected as artifact instead of a real object. Resolution characterization will be performed to provide substantial evidence to our results. We will look at two lasers: a 800-nm titanium:sapphire (Ti:S) laser (Mira 900, Coherent) and a custom 1060-nm ytterbium (Yb) fiber laser [21]. With the two lasers, we will investigate resolution based on PSF fitting with respect to depth in both *in vitro* and *in vivo* turbid samples; resolution with respect to laser type; and signal transmission through highly scattering media as related to laser type. Through PSF and signal propagation analysis, we will provide definite limits to the physiological items seen using our 2P imaging system.

Chapter 2

In Vitro PSF Measurements

To understand of how turbidity and depth influence resolution, we first looked at PSF characteristics in different *in vitro* samples. Phantom samples were made with varying intralipid levels to mimic the scattering properties of brain tissue. In the following experiments, we attempted to determine which phantom sample was most similar to brain tissue through investigating fluorescent signal decay. After determining decay rates, we then investigated the effects of depth on the measured PSF width under experimental conditions similar to those used for deep imaging. Phantom samples allowed us to not only draw conclusions from optical properties similar to those in mouse brain, but also with the *in vitro* samples, we investigated whether PSF trends differed as a function of depth, under various, controlled scattering characteristics, or with different laser illumination sources.

2.1 Microscope Setup

Both the Ti:S laser and the Yb laser tested were used independently with the same upright custom microscope [16]. Laser light was scanned using xy-galvanometer mirrors (6125H, Cambridge Technologies) through a scan

lens (SLP250, Thorlabs), a tube lens system (2 AC508-400-C lenses in a plossl design, Thorlabs), and an objective (XLUMPLFLN 20x 0.95 NA, Olympus) to the sample. Heavy water was used at the objective-sample interface to minimize the amount of light scattering. From the sample, fluorescent light returned through the objective and was redirected using a dichroic mirror (FF775-Di01-52x58, Semrock) to a PMT (H10770PB-40, Hamamatsu Photonics) prefaced with a bandpass filter (FF01-609/181-25, Semrock). Data from the PMT was finally collected using a multichannel DAQ (PCI-6259, National Instruments), and images were reconstructed from PMT data using custom software. All images used in this study are 512 x 512 pixels and have been averaged over 3 frames to reduce noise.

2.2 Samples

Mice and phantom samples were prepared for experimentation. All animal procedures were approved by The University of Texas at Austin Institutional Animal Care and Use Committee. To prepare a mouse (C57, male, 25-30 g, Charles River) for imaging, a bilateral craniotomy was performed to replace a portion of skull with a glass window, leaving the dura mater intact. The mouse was then given a minimum of three weeks recovery time to allow any inflammation incurred during surgery to subside.

Phantom samples were made with 1.3% agarose, varying levels of intralipid, and fluorescent micro-spheres. Agarose gave the sample some rigidity, while the intralipid provided scattering to the sample. The micro-spheres mim-

icked point sources for both lasers used, as the diffraction-based lateral focal volume is expected to be about 400 nm and 530 nm for the Ti:S laser and the Yb laser, respectively. To investigate the microscope's resolution at various scattering levels, 0%, 0.5%, 1%, 2%, and 4% intralipid (Intralipid 20%, Baxter) phantoms were created. Red 200-nm fluorescent micro-spheres (FluoSpheres F8793, Thermo Fisher Scientific) were mixed into all phantoms prior to agarose setting to allow even particle dispersion. Phantoms were covered with water and stored in a refrigerator when not in use.

Initial investigation of the micro-spheres in the 0% intralipid phantom showed the micro-sphere number as well as signal intensity did not vary significantly in depths up to 2 mm during an imaging session performed with the phantoms.

2.3 Fluorescent Decay

Scattering and absorption in the sample cause an exponential decay of light over penetration depth [10]. Samples with higher turbidity have shallower light penetration, while in lower scattering samples, light can reach greater depths [10]. We aimed to investigate the amount of signal decay in different scattering levels to give us a better understanding of how much scattering is present in brain tissue.

2.3.1 Experiment

Fluorescent decay rates were first collected for both the mouse brain tissue and the intralipid phantoms. During 2P imaging, the mouse was anesthetized with 80% N2/O2 vaporized isofluorane and kept at 37 °C in a stereotactic apparatus. A 50-µL retro-orbital injection of fluorescein (F2456, Sigma Aldrich) was administered to allow fluorescent imaging of the brain vasculature. The laser was focused at the brain surface, and power was adjusted to provide sufficient signal-to-background for imaging. With laser power held constant for the remainder of the imaging session, 2P images were taken into the brain in 5-µm-sized steps until no fluorescent signal was present. Image stacks were taken with three different mice to take into account physiological differences in brain tissue. The same imaging process was performed with each of the intralipid phantoms to allow comparison between live tissue and phantom sample. Both laser types were tested to analyze differences in illumination.

2.3.2 Analysis

Vasculature images were analyzed to determine how fluorescent signal degrades through brain tissue. After removing pixels indicating saturation of the image detector (defined as pixels of maximum bit value), the top 1% of pixel intensity values were averaged for each vascular image. The natural logarithm of the mean top 1% intensity values were then taken, and the relationship between the intensity values and depth was found using least-squares

linear fitting. This process was performed on all three mice, and the slope values were averaged to give an estimate of the fluorescent signal decay in brain tissue.

For the phantom images, each micro-sphere was isolated from the background by looking for local maxima in each image's intensity values. The micro-spheres were then discarded if they contained any saturated pixels, so the fitting function would be more accurate. Additionally, the distance between local maxima and the roundness of the suspected micro-sphere was measured to ensure a single micro-sphere was being considered instead of close neighboring micro-spheres. A distance between local maxima less than 30 pixels caused both micro-spheres in question to be discarded. Roundness, a metric of how circular a two-dimensional object is, was also calculated:

$$R = \frac{4A\pi}{P^2} \tag{2.1}$$

where R is the roundness coefficient, A is the area of a binary object, and P is object's perimeter. In using this measure of roundness, a value of 1 is considered perfect circle, and values deviating from 1 suggest a reduction in how 'round' an item is. A 15x15 pixel box was drawn around the local maxima with the local maxima approximately centered in the box, and the intensity values were thresholded to create a binary 15x15 box where the top 20% of the pixel intensity values were considered signal and the remaining were background. Any micro-spheres with a roundness coefficient less than 0.85 were removed from processing.

From there, the remaining micro-spheres were fitted to a two-dimensional Gaussian function using a mixture of a moment method and least-squares (LS) fitting [1, 7]. The two-dimensional Gaussian is used to approximate light propagation from a point source:

$$f(x,y) = A\exp -(a(x-x_0)^2 + 2b(x-x_0)(y-y_0) + c(y-y_0)^2) \tag{2.2}$$

where A is the amplitude, x_0 and y_0 are the center indices, and a, b, and c represent 0.5 over the covariance matrix:

$$\begin{bmatrix} a & b \\ b & c \end{bmatrix} \tag{2.3}$$

The LS method attempts to find the parameters A, x_0, y_0, a, b, and c that minimize the sum of the residual squares, where the residuals represent the difference between the actual intensity value seen the image compared to the expected intensity value based on the two-dimensional fitting.

In an attempt to decrease computation time of the LS Gaussian fitting function, the moment method was used to find the Gaussian center points.

$$C_x = \frac{\sum_i \sum_j (x_i \times I_{ij})}{\sum_i \sum_j I_{ij}} \tag{2.4}$$

C_x defines the center, x_i describes the position, and I_{ij} is the intensity of a given pixel [7]. Once the center x and the center y were found, the values were introduced as the centers to the LS fitting function. From there, LS fitting was used to estimate only the remaining Gaussian parameters, as outlined in Figure 2.1.

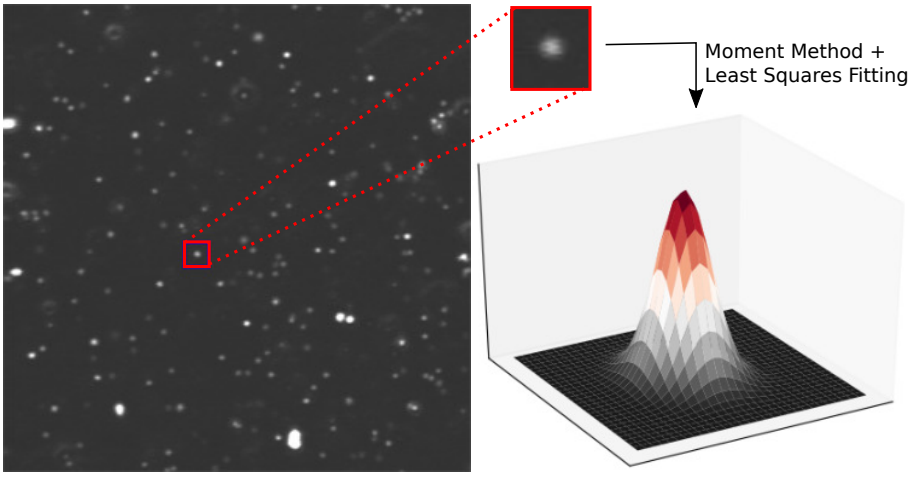

Figure 2.1: Micro-spheres are isolated from each image and then fitted to a two-dimensional Gaussian with a mixture of a Moment Method and LS Fitting

The fitted micro-sphere amplitudes were then averaged for each image, granted that at least 20 viable micro-spheres were counted. A plot of the average logarithm of micro-sphere amplitude as a function of depth was generated, and linear slopes were determined for each intralipid phantom to investigate fluorescent intensity decay.

2.3.3 Results

There are three noticeable portions of the signal decay in the brain: a large drop in signal near the surface, a signal decrease at a more linear rate, and a signal plateauing (Figure 2.2). Initially, the fluorescent signal near the surface is strong (Figure 2.2, bottom left panel). However, the signal decreases quickly, likely due to the intact dura mater [8]. Past the initial signal degradation, the logrithmic signal decay is linear until it reaches a steady state

plateau. Signal plateauing is due to the lack of adequate fluorescence and a dominance of background once the imaging limit is reached (Figure 2.2, bottom right panel). Because the penetration depth limitations often occur at points below the dura mater, we were interested in signal transmission through this area below, corresponding to approximately 100 µm to 200 µm in Figure 2.2.

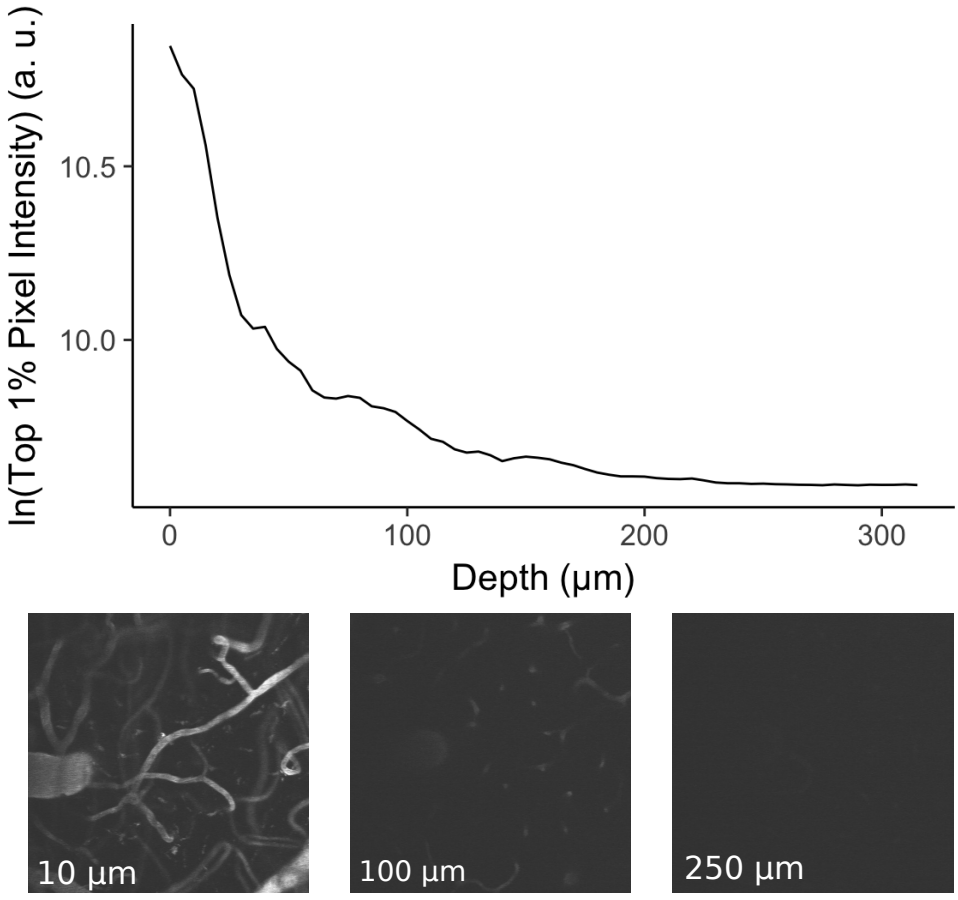

Figure 2.2: Fluorescent signal decay in mouse vasculature for single mouse imaged with the Ti:S laser

The mean slope of this area determined via linear regression for the

three mouse images was found to be -9.69 x10^{-4} µm^{-1} for the Ti:S laser and -4.27 x10^{-4} µm^{-1} for the Yb laser.

Unlike in the vasculature images, the logrithmic signal decay in the phantom images is linear due to consistent turbidity throughout each sample. To find the amount of signal decay in the phantoms, we were able to perform a simple linear regression on the mean logrithmic micro-sphere amplitude over depth for the entire phantom, instead of having to isolate a specific depth range. We compared the vasculature slopes to those found with the micro-spheres' amplitudes in the phantoms (Table 2.1).

Intralipid	Ti:S	Yb
0.5%	-5.02	-1.35
1%	-9.87	-4.50
2%	-18.4	-7.07
4%	-58.4	-37.2

Table 2.1: Slopes (x10^{-4} µm^{-1}) of logrithmic fitted intensity vs. depth

From this comparison, 1% intralipid seems to most closely approximate the scattering properties of mouse brain for both lasers. While signal decay in intralipid amounts greater than 1% suggests the phantoms do not mimic scattering properties, utilizing these phantoms to investigate resolution trends is useful, as we gain a better insight as to whether turbidity influences resolution.

2.4 PSF Width Measurements

Rather than maintaining the level of laser power incident on the sample, as with the fluorescent decay measurements, PSF widths were measured from images were the laser power was adjusted throughout the imaging experiment. Increasing the amount of laser power entering the sample as focal volume's depth increases reduces the amount of signal loss, meaning deeper imaging can take place. Mimicking the experimental protocols needed to maximize the depth of collected fluorescence gave us a better understanding of how resolution behaves further from the surface.

2.4.1 Experiment

Light scatters and is absorbed into the sample as the imaging depth is increased, causing the light that eventually reaches the detector to decrease exponentially with depth. Compensating for the decrease in signal by increasing the power of the light entering the sample allows deeper imaging. With the same phantom samples as described for fluorescent decay measurements, the incident laser power was increased using a half-wave plate as images were taken at greater depths to provide sufficient power levels during the entirety of the experiment [18].

2.4.2 Analysis

The same processing methods outlined above were performed to collect PSF characteristics for the micro-spheres. In the cases of the 2% and the

4% intralipid phantoms, the data from two sets of three-dimensional image stacks were combined together to increase the number of viable micro-spheres for processing. The x and y standard deviations were found and were then averaged. The full width at half the maximum (FWHM) value was calculated as 2.36 times the average of the two standard deviations [6]. These FWHM measurements are considered from this point on as the PSF's width.

Plots of mean width over depth were generated for all phantom types for each laser. Widths were compared for each intralipid concentration over depth, across intralipid amounts, and across laser types. The slopes of each plot were determined via linear regression to look for any significant resolution trends in the data. From there, the mean of all widths over all depths were compared between phantom types and between laser types using an ANOVA analysis. Through the investigation of each, we will gain a full understanding of how depth, turbidity, and wavelength influence resolution.

2.4.3 Results

Investigation of PSF width over depth is shown in Figures 2.3 and 2.4 for the Ti:S laser and in Figures 2.5 and 2.6 for the Yb laser. In each of these plots, points represent the mean of at least 20 PSF widths. Gaps in plot points are indicative of fewer than 20 individual micro-spheres being isolated for fitting. The standard deviation between widths are represented by vertical error bars. The y-axes are scaled the same for phantoms in their respective laser type; however, the x-axes are scaled differently for ease of data

visualization.

From the plots of mean micro-sphere widths, there is no significant degradation in resolution as depth is increased. This is exemplified through the data's slopes, where none are greater than $6x10^{-4}$ μm^{-1} for the Ti:S laser or $1x10^{-4}$ μm^{-1} for the Yb laser.

To investigate resolution relationships with intralipid and with laser type, the total width means for each intralipid amount and for both laser types were found (Table 2.2). Each value in the table represents the mean of all the mean micro-sphere widths collected for the specific sample, no matter the depth.

Intralipid	Ti:S	Yb
0.5%	0.933	0.945
1%	0.932	0.938
2%	0.937	0.938
4%	0.942	0.948

Table 2.2: PSF widths (µm) averaged across the range of depths imaged

The widths in all intralipid types for both lasers are around 0.93 to 0.94 µm. These values seem to be in line with the theorectical 2P FWHM widths of 0.88 µm for the red micro-spheres used in our phantoms [24].

Both our ANOVA tests on the varying intralipid phantoms suggest that is not a statistically significant difference between the average width of the micro-spheres embedded in any intralipid concentration tested (with p-values

of 0.17 and 0.10 for the Ti:S and the Yb laser, respectively).

When performing an ANOVA on the overall widths across all intralipid amounts and depths for each laser type, a p-value smaller than 0.05 (p-value = 0.0014) suggests that there is a significant difference between the PSF measurements of each laser type.

2.5 Discussion

Our *in vitro* phantom tests between varying turbidity provide a number of conclusions relevant to the resolution investigation. Firstly, the amount of turbidity generated with 1% intralipid in our phantom samples seems to most closely match that of mouse brain tissue for both laser types. This discovery gives us an understanding of which phantom would be appropriate for use in future *in vivo* investigations.

In measuring the PSF, there was no evidence of a large decrease in resolution (increase in PSF width) as a function of depth. In 0.5% intralipid phantoms, widths up to 1 mm with the Ti:S laser and up to 2 mm with the Yb laser were measured (although only 1 mm depths are shown for both lasers) and maintained size similarities. No changes in width measurements were seen for any intralipid phantoms. The trend not only indicates that optical resolution is not dependent on material properties, but suggests that in a more sample with greater heterogeneous turbidity, such as brain tissue, there should not be any changes in resolution in the different tissue types.

Although both laser types produced images with PSF widths similar to the estimated theoretical value of 0.88 [24], the PSF widths were not found to be the same. The Ti:S averages centered around 0.942 µm, while the Yb width means were around 0.936 µm. One possible reason for the discrepany between the two lasers is that the Ti:S laser produces visibly noisier images. Increases in noise have been shown to decrease the accuracy of fitting functions [1]. Regardless, both laser types produced images with PSF widths similar to the estimated theoretical value of 0.88 [24], with an error of about 7% and about 6% for the Ti:S and the Yb lasers, respectively.

One note to make about isolating the micro-spheres at greater depths is that the signal produced by the micro-spheres would not be enough to isolate accurately. This led to fewer numbers of micro-spheres being isolated deeper in the phantom samples, especially for the samples with greater amount of intralipid. Also, we did notice that noisier background signal levels produced large Gaussian fit inaccuracies. While maintaining sufficient signal levels for PSF width fitting in these experiments, we did not give a full analysis of how signal propagation behaves in brain tissue. The following chapter aims to outline how signal, background, and noise relate *in vivo* to give us an understanding of the true limits of resolution.

2.6 Conclusions

All being said, we did not find significant difference in resolution for the Ti:S or the Yb laser between intralipid amounts as found by measuring the PSF

width. There was a statistically significant difference in the resolution between the two lasers, but the widths were about 0.006 µm different. From this, we can conclude that the PSF width is not heavily influenced by environment or excitation source, as long as adequate signal-to-noise is achieved.

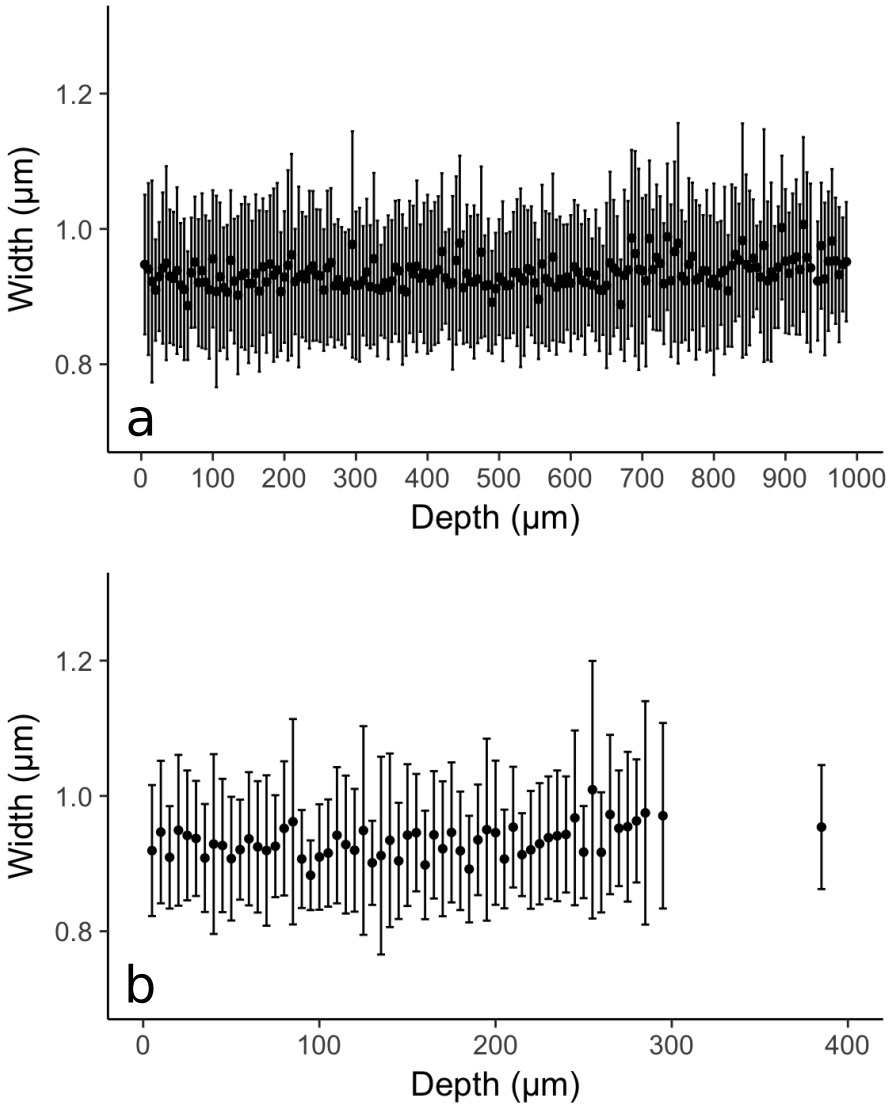

Figure 2.3: Mean micro-sphere widths for phantoms with (a) 0.5% intralipid and with (b) 1% intralipid recorded using the Ti:S laser

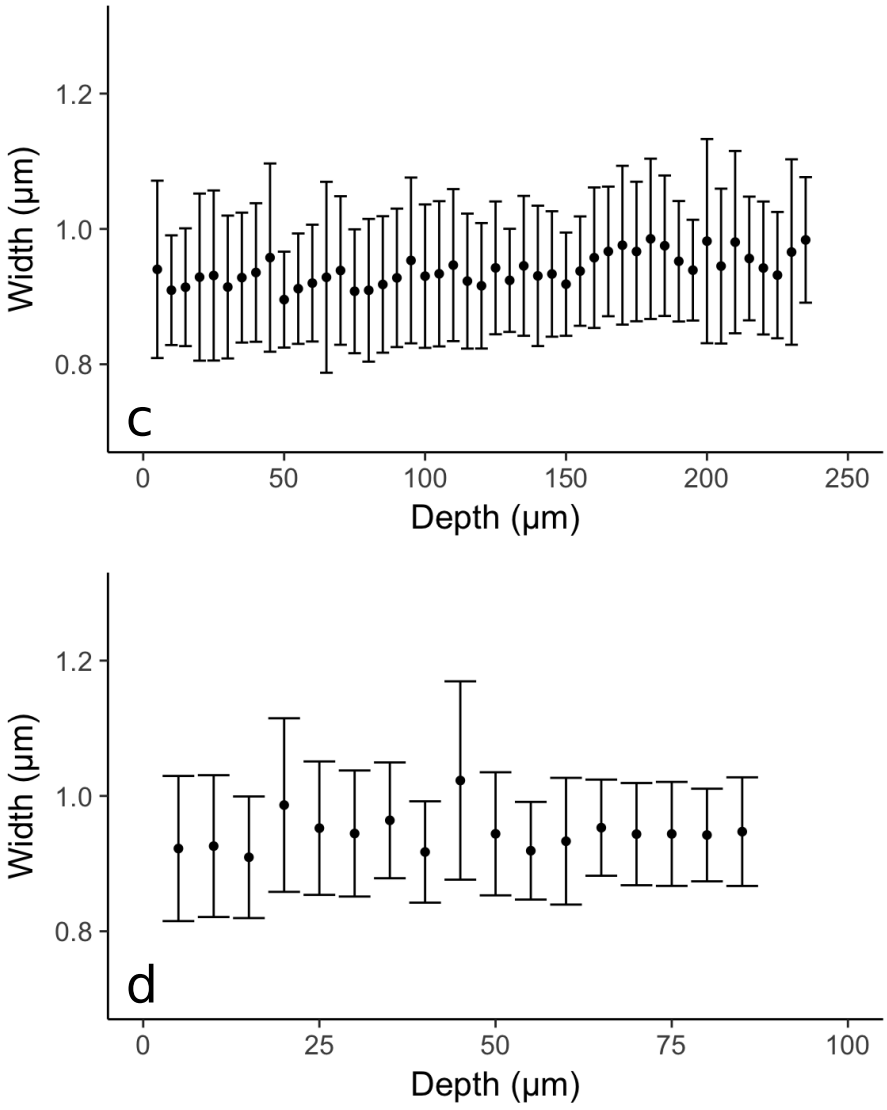

Figure 2.4: Mean micro-sphere widths for phantoms with (c) 2% intralipid and with (d) 4% intralipid recorded using the Ti:S laser

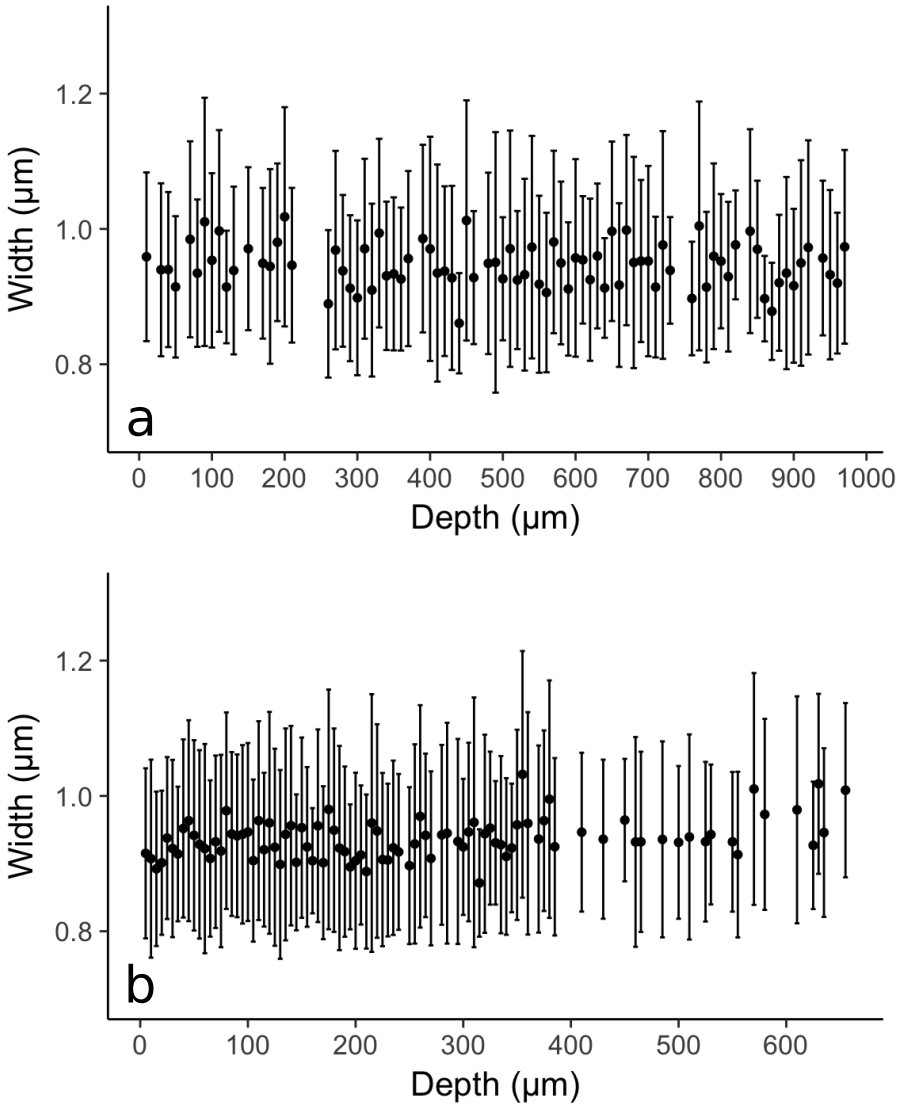

Figure 2.5: Mean micro-sphere widths for phantoms with (a) 0.5% intralipid and with (b) 1% intralipid recorded using the Yb laser

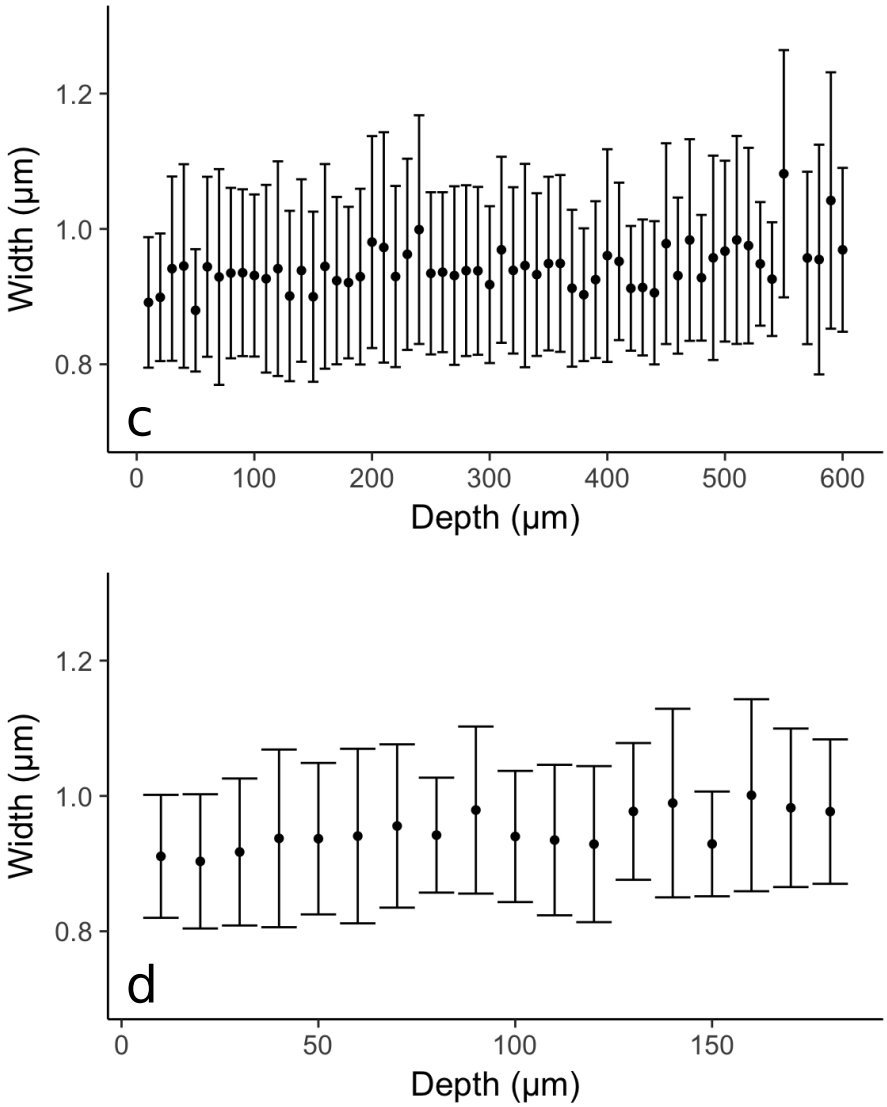

Figure 2.6: Mean micro-sphere widths for phantoms with (c) 2% intralipid and with (d) 4% intralipid recorded using the Yb laser

Chapter 3

Line Scans

Investigating line scan measurements allowed us to determine how signal, background, and noise change as a function of depth *in vivo*. Line scanning to collect blood flow measurements is a process where the 2P laser beam is scanned repetitively back and forward along a vessel filled with fluorescent dye. Intensity values are collected during the scanning process and are reconstructed to give an image representing the intensities through the line scan distance with respect to the time over which the scans were performed (Figure 3.1). If the vessel is small enough, individual blood cells can be seen as dark bands in the line scan as the cells do not absorb the dye injected into the vasculature, and the remaining plasma is seen as bright signal. Flow measurements can then be made to measure how the individual cells move through the vessel over time [4].

For our studies, we will instead be looking at the relationship between the plasma region ('signal') and the cell region ('background') in line scan measurements. We will also investigate how noise changes over the same conditions. All line scan points are located in a small region, making it useful for signal and background comparisons because things such as out-of-focus fluo-

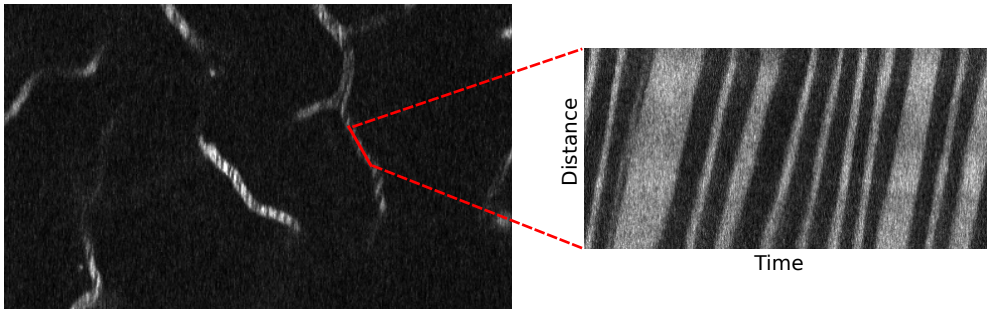

Figure 3.1: A 2P image and the resulting line scan

rescence and vignetting will not uniquely impact intensity values. As with any signal attenuation *in vivo*, the intensity of signal compared to the intensity of background changes with respect depth (Figure 3.2). By comparing signal, background, and noise over a variety of depths, we will see how the signal-to-background and signal-to-noise (SNR) are impacted as images are taken at deeper levels. As with our other experiments, both the Ti:S laser and the Yb laser will be used to investigate how wavelength influence signal propagation.

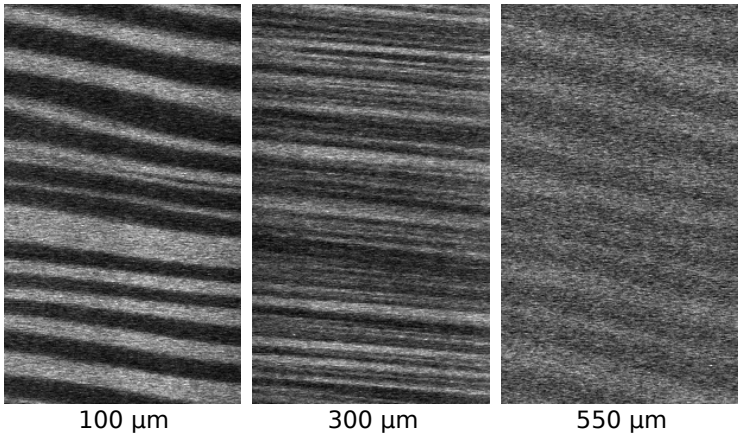

Figure 3.2: The contrast of the line scans changes with respect to depth

3.1 Experiment

Line scans were collected from an anesthetized mouse. The cranial window insertion and the anesthetization process follow the same protocol as was outlined in Chapter 2. To cause fluorescence in the vasculature, a 100-µL retro-orbital fluorescein injection was administered to provide fluorescent signal in the vessels when imaging with the Ti:S laser; a 100-µL retro-orbital Texas Red (A2348, Sigma Aldrich) injection was performed for the Yb laser. At each depth, line scans were performed such that 200 back-to-back scans were taken at a rate of 450 kHz along a minimum of three vessels. Vessels were chosen based on their size and their curvature: blood cells are generally easier to see in small vessels and straight segments are easier to scan the laser beam across. Laser power was increased with depth to compensate for the exponential signal drop off that occurs in brain tissue. Line scans were performed at increasing depths until signal could no longer be distinguished from the background.

3.2 Analysis

Analysis of the line scan data was used to collect information about signal quality *in vivo*. Line scan images with portions of the scan that fell outside the vessel or images that did not have any intensity distinction between signal and background were removed from image analysis. For pre-processing, the angle at which the blood cell lines were moving across the line scan was found from the radon transform. The image was then rotated to compensate

for the cell line angle such that the final line scan image was a series of bright and dark horizontal lines. Contrast, signal, and background measurements described below were found using the average of ten equally spaced vertical intensity profiles along the rotated line scan image, ignoring the black border added during the rotation process (Figure 3.3).

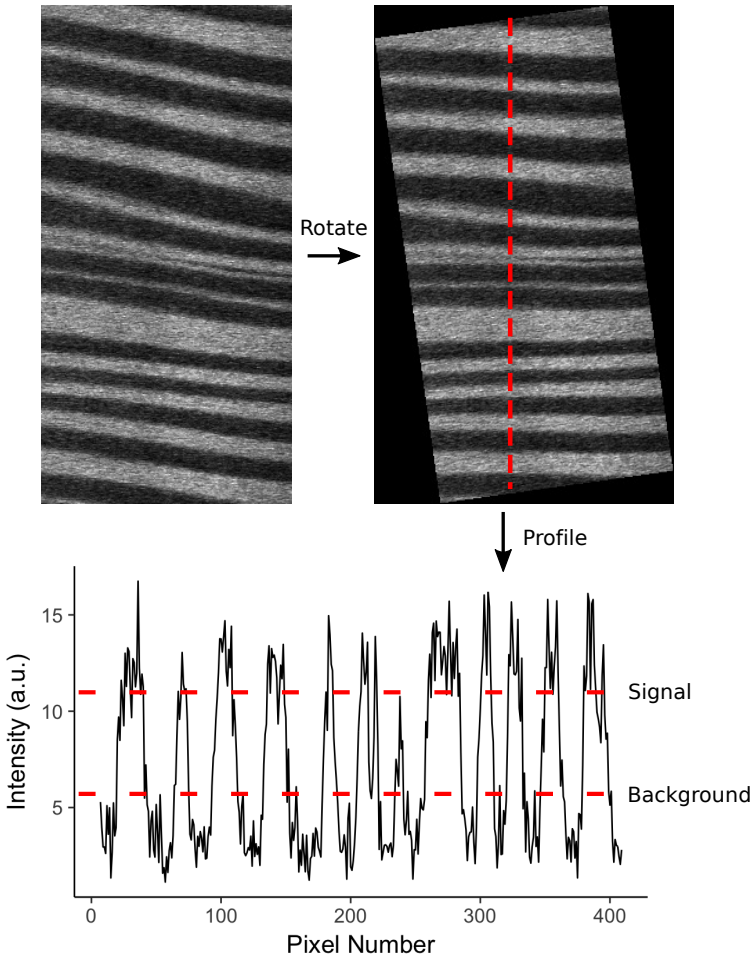

Figure 3.3: A sample profile taken from the rotated line scan image, along with threshold values for signal and background

Contrast, or the difference between the signal intensity and the background intensity, was measured as:

$$C = \frac{max[I] - min[I]}{max[I] + min[I]} \tag{3.1}$$

where C is the contrast value, $max[I]$ is the maximum intensity value of the line, and $min[I]$ is the minimum intensity value of the line. The contrast values across the line scans were averaged for each depth, and a plot of the mean contrast over depth was created.

Additionally, the components that contribute to contrast, the signal and background regions of the line scan image, were investigated. Signal was defined as the brightest 30% of pixels in the line scan, with saturated pixels excluded. Background was defined as the darkest 30% of the pixels. By looking at only the extreme regions of the pixel intensity range, we were able to ensure that minimal signal was labeled as background or vice versa. For both the signal and the background, values were averaged across the line scans for all depths.

Lastly, the amount of noise for each image was quantified. To do this, the standard deviation of the background pixels for the entire 512 x 512 image plane that the vessel used for the line scan was found. Mean standard deviation values were found and compared over depth.

3.3 Results

Contrast, signal, background, and noise plots for the Ti:S laser are shown in Figures 3.4 and 3.5 and for the Yb laser in Figures 3.6 and 3.7. In the plots, data points are the mean values across line scans. Error bars indicate the standard deviation between line scans. The dashed gray line depicts the least-squares linear regression line associated with the data. The x-axes are scaled with respect to laser type; the y-axis for each plot is not specifically scaled.

For each data set, the Pearson correlation coefficient was determined between data type and depth to investigate the strength of the linear relationships. Values for the correlations as well as their corresponding p-values are shown in Table 3.1.

	Ti:S		Yb	
	corr	p-value	corr	p-value
Contrast	-0.922	0.0001	-0.894	0.0005
Signal	0.336	0.3418	-0.429	0.2156
Background	0.869	0.0011	0.709	0.0217
Noise	0.826	0.0033	0.649	0.0421

Table 3.1: Pearson correlation coefficients

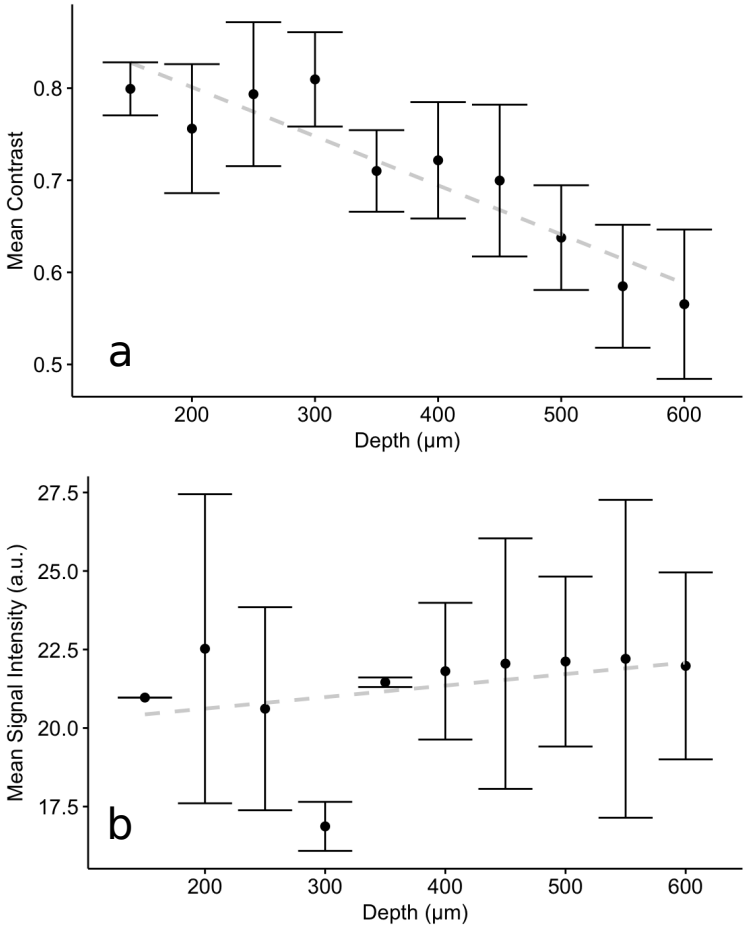

Figure 3.4: (a) Contrast and (b) average signal intensity of line scans taken using the Ti:S laser

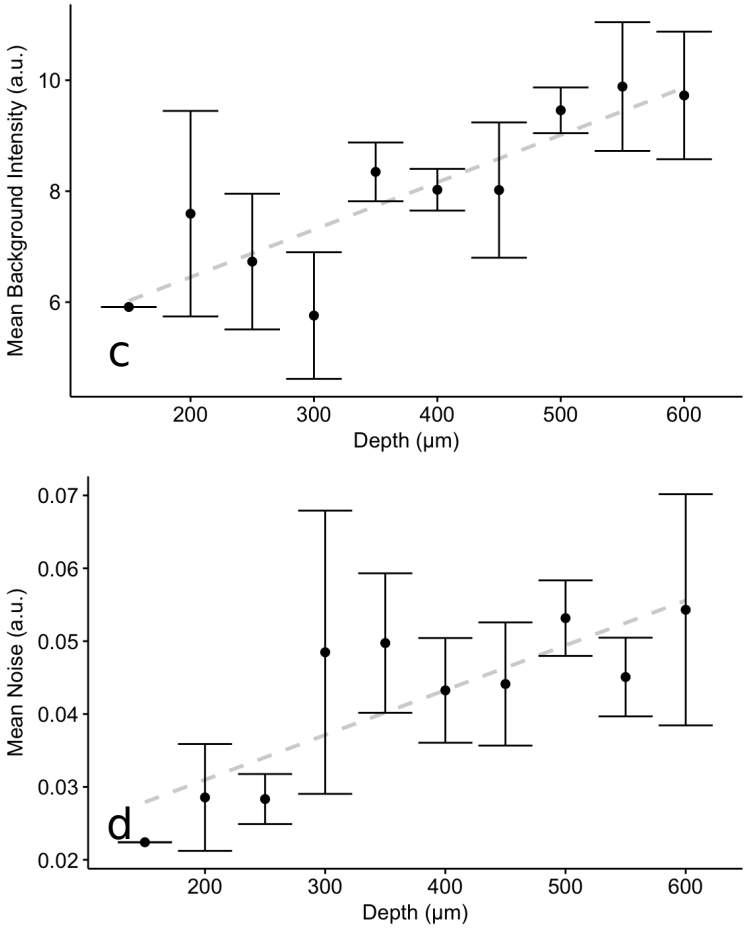

Figure 3.5: (c) Average background intensity and (d) average noise taken using the Ti:S laser

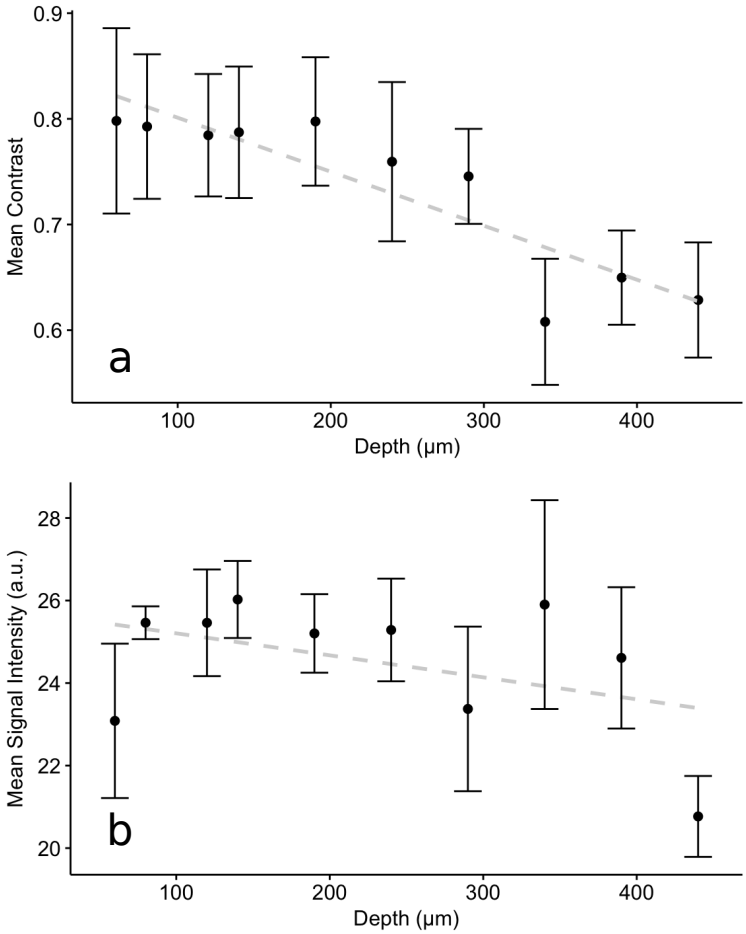

Figure 3.6: (a) Contrast and (b) average signal intensity of line scans taken using the Yb laser

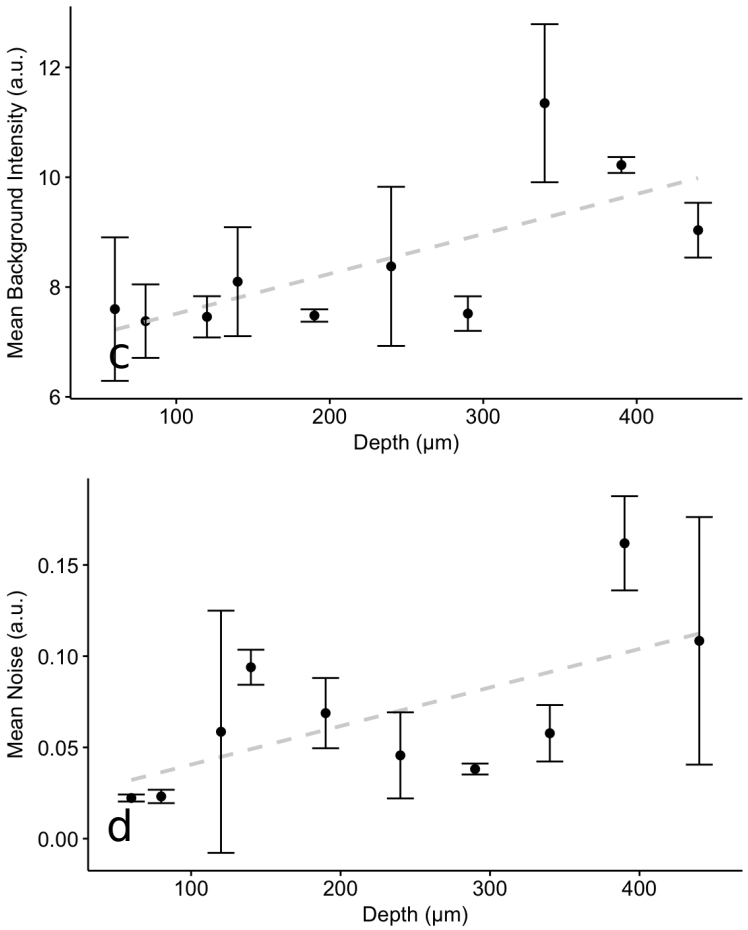

Figure 3.7: (c) Average background intensity and (d) average noise taken using the Yb laser

3.4 Discussion

Determining a correlation coefficient for each analytic measure, the contrast seems to have significant evidence (p-value less than 0.05) that indicates that there is a strong, negative linear relationship between contrast and depth. The signal intensity, with a p-value much greater than 0.05, suggests that the null hypothesis that there is zero correlation between the two should not be rejected; there is no real correlation between signal intensity and depth. The lack of relationship is reasonable, as the laser power is adjusted to allow greater penetration depth. When looking at the background intensity and noise, however, we see a positive correlation between the background and depth and noise and depth, as both conditions have positive correlation coefficients and small p-values. These trends were seen when using both laser types, indicating that excitation wavelength does not change the overall fact that contrast, background intensity, and noise change with respect to depth.

Degradation of background signal is potentially caused by the high turbidity of the brain tissue. Studies have shown that when the scattering coefficient of a sample reaches at least 1.4 mm^{-1}, fluorescent light originally excited at the focal volume scatters so much before exiting the surface of the sample that more fluorescent signal is present toward the surface than is present at the focal volume [32]. The movement of the fluorescent light outside of the focal volume could cause the overall background to appear brighter as the focal volume is shifted out of the imaging plane. This trend is exacerbated as the imaging depth in increased [32]. Brain tissue has greater scattering coeffi-

cients than 1.4 mm^{-1} [5], indicating that there are likely some high scattering events occurring in sample. All this means that the fluorescence generated by 2P excitation in highly turbid samples could be more distributed outside the focal volume and could lead to messier images.

The background increase as well as the noise increase with depth also suggest that there may be difficulty determining PSF widths at great depths. Because background intensity increases, thus leading to a decrease in contrast, there is difficulty distinguishing fluorescent items in a sample from the background. This was seen in with the micro-sphere measurements in Chapter 2, where low signal-to-background distinction prevented many micro-spheres from being isolated. Additionally, the increase in noise with the signal maintenance indicates that the SNR decreases with depth. The decay suggests that fitting functions may become less accurate as depth increases [1]. Overall, the changes in background and in noise over depth could lead to inaccuracies in PSF fitting as the depth limit is reached.

It is worth noting the difference in penetration depth between the Ti:S laser and the Yb laser. Because longer wavelengths penetrate more deeply into biological tissue [20], we would expect the Yb laser to allow deeper imaging when performing line scans. This discrepancy is partially due to the Yb laser pulse width used for line scans. Unlike for remaining chapters, where the pulse with was measured to be around 120 fs, the pulse width for the Yb laser when performing the line scans was measured at 221 fs. The broadening of the pulse width has been shown to influence both image quality and depth [26,28]. Also,

the age of the mice used for imaging likely had effects on the imaging depth. The mice imaged with the Yb laser were much older than those images with the Ti:S laser. Research has shown that mature mice have greater attenuation of the fluorescent signal generated when using 2P imaging [20]. Both these likely affected the imaging session, as we noticed a sharper decrease in signal intensity over depth. No matter the pulse width or the mouse's age, however, the same trends between signal and background were seen in all mice and both laser types used.

3.5 Conclusions

In this section, we investigated how contrast, signal, background, and noise change as a function of depth. We controlled laser power into the sample to maintain signal values. Doing this, we saw a decrease in contrast and an increase in both background intensity and noise as we took images at greater depths. Because contrast is a function of signal intensity and background intensity, the degradation in background lead to the decrease in contrast. The trends all indicate that in deep imaging experiments, signal-to-background and SNR decrease with imaging depth. These decreases are likely to degrade image quality and make image analysis difficult.

Chapter 4

In Vivo PSF Measurements

Investigating the PSF width in mouse brain tissue will give the final conclusion of how resolution changes based on depth *in vivo*. Because the potential biological items in the brain available to approximate a point source are either too abundant to isolate at the 2P expected resolution or have sizes with a range that spans above and below the point source size requirement [15,33], we attempted to insert fluorescent micro-spheres into the brain directly. Experimental procedures similar to those used for deep imaging were then utilized to collect images. *In vivo* samples allowed us to draw conclusions about how the heterogeneous properties of brain tissue affect PSF width.

4.1 Samples

Micro-spheres were injected into the mouse brain during the cranial window process so they could diffuse into the brain tissue. First the skull was removed. A 1-mm diameter glass capillary was pulled, cut at its tip to allow fluid flow, and attached to a micro-injector (NANOLITER2010, World Precision Instruments) for tissue injections. The glass capillary was inserted 1050 µm into the brain tissue and was then moved toward the brain surface

by 50 µm. A 9.2 nL volume of micro-spheres was injected into the tissue at that point. Injections were performed every 50 µm in this manner until the capillary was situated at the brain surface. Anywhere from one to three injection sites were used for each mouse. All injection sites were placed near vascular branch points and were photographed, so they could be found again during experimentation. After injections, the cranial window was attached, and the mouse was given a minimum of three weeks to recover.

The injection process was not as effortless as originally thought. In almost all mice injected, the micro-spheres would be largely collected near the brain surface, with few individuals at larger depths (Figure 4.1).

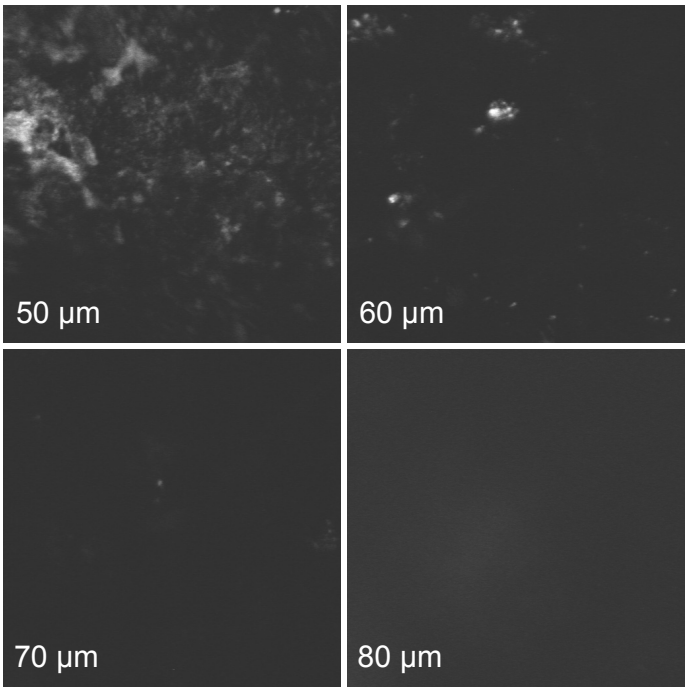

Figure 4.1: Beads collect at the surface of *in vivo* samples

Furthermore, in select mice we would see cellular bodies filled with fluorescent material toward the surface of the brain (Figure 4.2). In certain cases, the granular items in the cells looked like the micro-spheres used for injections.

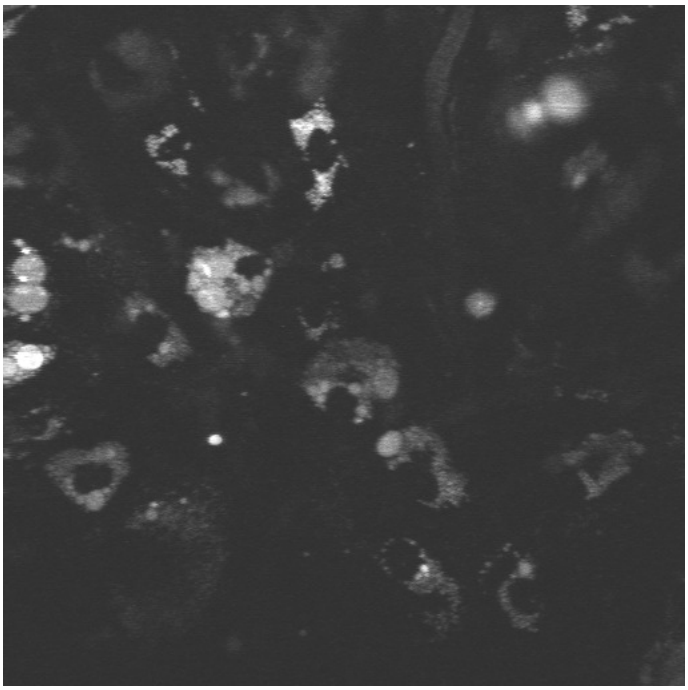

Figure 4.2: Cells at the brain surface appear to have engulfed fluorescent material

In the end, we were not able to perform injections in which a large number of micro-spheres were present for PSF width analysis. We could not find evidence in our samples of micro-spheres residing at depths greater than about 300 µm below the brain surface. Regardless, a small number of individual micro-spheres were isolated from experimental images. *In vivo* width

analysis was performed using the Ti:S laser on these samples. With the results, we began to get an idea of how the PSF width is influenced in living tissue.

4.2 Experiment

For imaging, the micro-sphere-injected mouse was anesthetized and placed in a stereotactic frame. A laser speckle image was taken of the brain surface to make a map of the surface vasculature using a 785-nm laser diode (L785P090, Thorlabs) and a camera (acA2040-90umNIR, Basler) attached adjacent to the 2P microscopy setup [2]. Also, a 50-µL retro-orbital injection of fluorescein was administered, and 2P images, with a smaller field-of-view, were taken of the surface vessels. The laser speckle image and the 2P vasculature images were then compared to the images taken during the craniotomy to help position the mouse near the injection location.

Once an injection site was located, we used similar experimental processes to those used for determining the PSF widths in the phantom samples. Laser power was adjusted to compensate for signal decay as images were taken in 1 µm steps into the tissue sample in locations adjacent to the injection path.

4.3 Analysis

Because 1 µm steps were taken, single micro-spheres would appear in multiple images. To avoid a micro-sphere being counted more than once, the

isolation portion of the analysis was modified to choose local maxima over three-dimensions. Similar analysis for determining a single micro-sphere and for fitting the PSF width was performed as was outlined in Chapter 2.

Because too few micro-spheres were found during imaging to provide a minimum of 20 micro-spheres for averaging, the widths were averaged for whatever number of micro-spheres were found. The widths were then plotted across depth. The slope of the linear regression between width and depth was measured to determine whether there was a trend between the two. The mean *in vivo* width was then compared to the Ti:S laser *in vitro* widths found using the phantoms.

4.4 Results

The PSF widths found for brain tissue are shown in Figure 4.3. No standard deviation bars are present because there were many instances where only one micro-sphere was found at a specific depth.

Because the slope of the linear regression between the width and depth was small ($9x10^{-4}$ μm^{-1}), we determined there was no real trend between width and depth. The average of the micro-spheres across all depths was 1.03 µm, larger than the mean width for all intralipids foun with the Ti:S laser of 0.936 µm. The width we would expect given the micro-sphere is 0.88 µm [24].

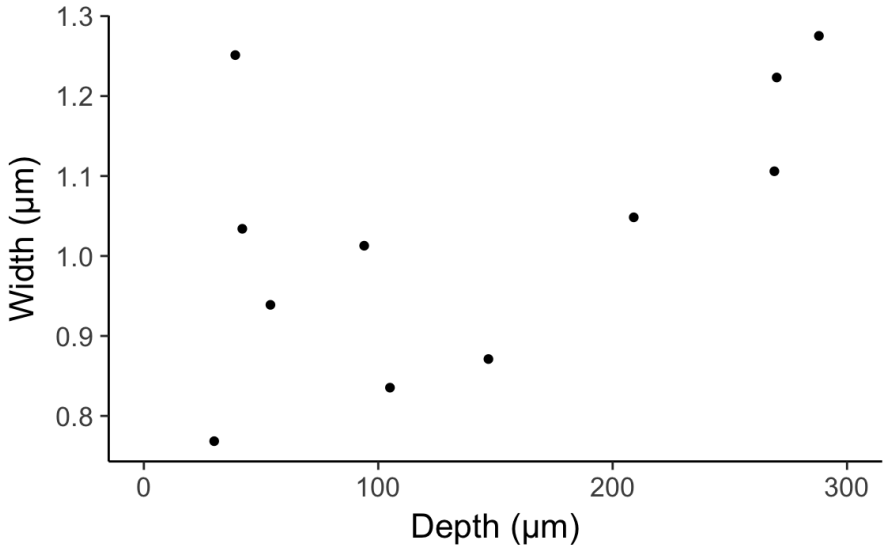

Figure 4.3: Micro-sphere widths for *in vivo* mouse brain tissue recorded using the Ti:S laser

4.5 Discussion

Our goal of inserting numerous micro-spheres into mouse brain up to the imaging depth limit was not achieved. Instead, we encountered many difficulties that reduced the number of micro-spheres we had for resolution measurements. Firstly, micro-spheres had congregated around the exterior of the injection site in many of our samples. This issue was present no matter the number of micro-spheres injected (from 4,000 micro-spheres per total injection to 400,000 micro-spheres per total injection). The superficial collecting at all injection numbers suggests that the micro-spheres had moved back up through the injection site toward the surface instead of diffusing into the brain tissue. Micro-sphere congregation would not be devastating, had there been

enough individual micro-spheres to isolate and fit. However, the micro-sphere congregation in many cases made them indistinguishable from one another.

In the initial injections, we used the same 200-nm carboxylate micro-spheres we had used for the phantom samples, as the micro-spheres were bright and easy to fit. The properties of these micro-spheres, however, turned out not to be ideal for tissue diffusion. In the phantoms, micro-spheres simply needed to be suspended in agarose for sufficient imaging. However, brain tissue contains winding, narrow spaces between cell membranes that the micro-spheres need to spread through. The amount of diffusion has been seen to be limited by extracellular space (ECS) tortuosity and by particle interactions with cell walls [27]. Groups have suggested that particles smaller than 100 nm and with a positively-charged coating would have the greatest chance of diffusing away from the injection site into the ECS of the mouse brain [19,31]. For future injections, smaller, streptavidin-coated micro-spheres may provide better diffusion and reduce the amount of surface collection.

Another issue was the microsphere filled cells, resembling macrophages, seen in some of the mouse samples. Macrophages in *in vivo* systems clear cell debris and foreign bodies from a host [12,22]. In the case of the microspheres, macrophages could have potentially reduced the number present for imaging. Using a coating that would make the micro-spheres 'invisible' in the brain could minimize the chances of macrophages collecting the microspheres [12]. Additionally, imaging sooner so the mouse's immune response is not yet activated could reduce the number of macrophages [12]; although tissue inflammation

due to the craniotomy may be present.

One final possibility for increasing the number of micro-spheres in brain tissue is to use a different injector. Other groups have injected similar micro-spheres to measure PSF in living tissue with a pressurized injector [11, 29] rather than an injector that uses a fine-tuned plunger to move liquid out of a capillary. With a pressurized injector, the liquid volume is injected with pressurized air [13] that forces the liquid into the sample. Diffusion may be more likely with the liquid moving into the sample with greater force.

Despite the troubles we experienced preparing *in vivo* samples, we were able to collect some PSF width data in living mouse brain with the Ti:S laser. Results indicate the PSF width in tissue is about 1.03 µm and there is no significant change in width up to 288 µm. This width is slightly larger than both the mean width of 0.936 µm for all intralipids found with the Ti:S laser and the expected width produced from the red micro-spheres of 0.88 µm [24]. Differences could be due to the increased noise of the *in vivo* environment compared to the phantom samples. Further, the small number of micro-spheres used for fitting likely reduced the overall accuracy of the results, as the number of samples needed to represent the population was not reached.

4.6 Conclusions

For future mouse brain injections, the goal should be to increase the number of individual micro-spheres present for isolation. Smaller micro-spheres with streptavidin coating could be tried to increase the amount of diffusion into

the tissue. A pressurized injector may also be useful in increasing diffusion in tissue. If the presence of macrophages is a concern, imaging closer to the time of injection could reduce the chances of the cells eliminating micro-spheres.

In the end, our results showed a slight difference between the PSF width *in vivo* and *in vitro*, with the *in vivo* width being larger. We can speculate that there will likely not be a change in resolution as a function of depth in the mouse brain, although more data would need to be collected to confirm these specific findings.

Chapter 5

Conclusions

The goal of our research was to investigate resolution and signal of our 2P imaging system as a function of depth. Through our experiments, we investigated resolution based on PSF fitting with respect to depth in both *in vitro* and *in vivo* samples, determined resolution with respect to laser type, and investigated signal transmission through highly scattering media with respect to depth. Through this, we provide a better understanding of physiological size limitations that can be investigated with our 2P microscope.

To determine resolution of our 2P microscope, we used 200 nm microspheres to mimic point sources and found the widths of the PSF to measure resolution. Using our *in vitro* samples, we determined our resolution to be about 0.942 µm for the Ti:S laser and 0.936 µm for the Yb laser in intralipid phantom samples. These values were fairly close to the theoretical PSF width of 0.88 µm, giving us errors of 7% and 6% for the Ti:S laser and the Yb laser, respectively. These tests suggested little difference in the resolution when using either laser type or when looking at increased levels of scattering in our samples in depths throughout the imaging range.

For the *in vivo* samples, we found the resolution to be a little larger,

about 1.08 µm, giving a 23% error from the theoretical resolution. Although we were only able to measure our *in vivo* samples with the Ti:S laser, the similarities between the resolution measurements for both laser types with the *in vitro* samples suggests that there will not be a large difference in resolution *in vivo* for the Yb laser.

For further experimentation, finding better methods to create *in vivo* samples will be necessary. Although we were able to isolate a handful of micro-spheres in our mouse samples, more would need to be used to create confident results. Change in micro-sphere coatings and size as well as a different injection tool could prove fruitful in future studies. Either way, nothing in our current studies suggest that 2P resolution has either *in vitro* or *in vivo* depth dependencies.

To investigate the signal propagation, we collected vasculature line scans over a variety of depths in mouse samples. Through maintaining signal intensity over depth, we saw a decrease in the contrast of our line scans over depth, as well as an increase in background intensity and in noise. Increase in background and the decrease in contrast hint that the decrease in image quality over depth may be due to the inability to distinguish between signal and background. Further, the increase in noise in the sample suggests a decrease in overall SNR as images are taken deeper in the mouse sample. Relating to the PSF measurements, changes in PSF width calculated via LS could be partially attributed to the increase in noise as noise impacted the LS fitting function. Both these trends, as well as the resolution measurements we per-

formed, suggest that the challenges faced when using 2P microscopy at deep depths will likely be due to signal propagation trends and not to the decrease in resolution.

Bibliography

[1] Stephen M. Anthony and Steve Granick. Image analysis with rapid and accurate two-dimensional Gaussian fitting. *Langmuir*, 25(14):8152–8160, 2009.

[2] David A. Boas and Andrew K. Dunn. Laser speckle contrast imaging in biomedical optics. *Journal of Biomedical Optics*, 15(1):011109, 2010.

[3] Born and Wolf. Principles Of Optics (ref5). page 859, 1970.

[4] Emmanuelle Chaigneau, Martin Oheim, Etienne Audinat, and Serge Charpak. Two-photon imaging of capillary blood flow in olfactory bulb glomeruli. *Proceedings of the National Academy of Sciences of the United States of America*, 100(22):13081–6, 2003.

[5] Wf F Cheong, S.a. Sa Prahl, and a.J. Aj Welch. A review of the optical properties of biological tissues, 1990.

[6] Author J J Condon. Errors in Elliptical Gaussian Fits. 109(732):166–172, 2018.

[7] John C. Crocker and David G. Grier. Methods of Digital Video Microscopy for Colloidal Studies. *Journal of Colloid and Interface Science*, 179(1):298–310, 1996.

[8] Ilaria Decimo, Guido Fumagalli, Valeria Berton, Mauro Krampera, and Francesco Bifari. Meninges: from protective membrane to stem cell niche. *American journal of stem cells*, 1(2):92–105, 2012.

[9] A K Dunn, V P Wallace, M Coleno, M W Berns, and B J Tromberg. Influence of optical properties on two-photon fluorescence imaging in turbid samples. *Applied Optics*, 39(7):1194–1201, 2000.

[10] X. S. Gan, S. P. Schilders, and Min Gu. Image formation in turbid media under a microscope. *Journal of the Optical Society of America A*, 15(8):2052, 1998.

[11] Olga Garaschuk, Ruxandra Iulia Milos, and Arthur Konnerth. Targeted bulk-loading of fluorescent indicators for two-photon brain imaging in vivo. *Nature Protocols*, 1(1):380–386, 2006.

[12] Heather Herd Gustafson, Dolly Holt-Casper, David W Grainger, Hamidreza Ghandehari, and David Grainger. Nanoparticle Uptake: The Phagocyte Problem HHS Public Access. *Nano Today*, 10(4):487–510, 2015.

[13] Parker Hannifin and Pine Brook. PICOSPRITZER ® III Manual & FAQ's PICOSPRTIZER® III Pressure Systems for Ejection of Picoliter Volumes in Cell Research OPERATING MANUAL.

[14] Fritjof Helmchen and Winfried Denk. Deep tissue two-photon microscopy. (December), 2005.

[15] Fang Huang, Samantha L. Schwartz, Jason M. Byars, and Keith A. Lidke. Simultaneous multiple-emitter fitting for single molecule super-resolution imaging. *Biomedical Optics Express*, 2(5):1377, 2011.

[16] S. M. Shams Kazmi, Anthony J. Salvaggio, Arnold D. Estrada, Michael A. Hemati, Nazariy K. Shaydyuk, Emannuel Roussakis, Theresa A. Jones, Sergei A. Vinogradov, and Andrew K. Dunn. Three-dimensional mapping of oxygen tension in cortical arterioles before and after occlusion. *Biomedical Optics Express*, 4(7):1061, 2013.

[17] Demirhan Kobat, Nicholas G. Horton, and Chris Xu. In vivo two-photon microscopy to 1.6-mm depth in mouse cortex. *Journal of Biomedical Optics*, 16(10):106014, 2011.

[18] David R. Miller, Ahmed M. Hassan, Jeremy W. Jarrett, Flor A. Medina, Evan P. Perillo, Kristen Hagan, S. M. Shams Kazmi, Taylor A. Clark, Colin T. Sullender, Theresa A. Jones, Boris V. Zemelman, and Andrew K. Dunn. In vivo multiphoton imaging of a diverse array of fluorophores to investigate deep neurovascular structure. *Biomedical Optics Express*, 8(7):3470, 2017.

[19] E. A. Nance, G. F. Woodworth, K. A. Sailor, T.-Y. Shih, Q. Xu, G. Swaminathan, D. Xiang, C. Eberhart, and J. Hanes. A Dense Poly(Ethylene Glycol) Coating Improves Penetration of Large Polymeric Nanoparticles Within Brain Tissue. *Science Translational Medicine*, 4(149):149ra119–149ra119, 2012.

[20] Martin Oheim, Emmanuel Beaurepaire, Emmanuelle Chaigneau, Jerome Mertz, and Serge Charpak. Two-photon microscopy in brain tissue: Parameters influencing the imaging depth. *Journal of Neuroscience Methods*, 111(1):29–37, 2001.

[21] Evan P. Perillo, Justin E. McCracken, Daniel C. Fernée, John R. Goldak, Flor A. Medina, David R. Miller, Hsin-Chih Yeh, and Andrew K. Dunn. Deep in vivo two-photon microscopy with a low cost custom built mode-locked 1060 nm fiber laser. *Biomedical Optics Express*, 7(2):324, 2016.

[22] V. H. Perry, D. A. Hume, and S. Gordon. Immunohistochemical localization of macrophages and microglia in the adult and developing mouse brain. *Neuroscience*, 15(2):313–326, 1985.

[23] S. Ram, E. S. Ward, and R. J. Ober. Beyond Rayleigh's criterion: A resolution measure with application to single-molecule microscopy. *Proceedings of the National Academy of Sciences*, 103(12):4457–4462, 2006.

[24] C. Sheppard and M. Gu. Image formation in two-photon fluorescence microscopy. *Optik*, 86(3):104–106, 1990.

[25] Andy Y. Shih, Jonathan D. Driscoll, Patrick J. Drew, Nozomi Nishimura, Chris B. Schaffer, and David Kleinfeld. Two-photon microscopy as a tool to study blood flow and neurovascular coupling in the rodent brain. *Journal of Cerebral Blood Flow and Metabolism*, 32(7):1277–1309, 2012.

[26] Karel Svoboda and Ryohei Yasuda. Principles of Two-Photon Excitation Microscopy and Its Applications to Neuroscience. *Neuron*, 50(6):823–839, 2006.

[27] Eva Syková, Charles Nicholson, and Charles Sykova, Eva; Nicholson. Diffusion in brain extracellular space. *Physiological reviews*, 88(4):1277–1340, 2008.

[28] Shuo Tang, Tatiana B. Krasieva, Zhongping Chen, Gabriel Tempea, and Bruce J. Tromberg. Effect of pulse duration on two-photon excited fluorescence and second harmonic generation in nonlinear optical microscopy. *Journal of Biomedical Optics*, 11(2):020501, 2006.

[29] Zachary J Taylor, Edward S Hui, Ashley N Watson, Xingju Nie, Rachael L Deardorff, Jens H Jensen, Joseph A Helpern, and Andy Y Shih. Microvascular basis for growth of small infarcts following occlusion of single penetrating arterioles in mouse cortex. *Journal of Cerebral Blood Flow & Metabolism*, 36(8):1357–1373, 2016.

[30] Patrick Theer, Mazahir T. Hasan, and Winfried Denk. Two-photon imaging to a depth of 1000 m in living brains by use of a Ti:Al_2O_3 regenerative amplifier. *Optics Letters*, 28(12):1022, 2003.

[31] Robert G Thorne and Charles Nicholson. In vivo diffusion analysis with quantum dots and dextrans predicts the width of brain extracellular space. *Proceedings of the National Academy of Sciences of the United States of America*, 103(14):5567–72, 2006.

[32] J Ying, F Liu, and R R Alfano. Spatial distribution of two-photon-excited fluorescence in scattering media. *Applied optics*, 38(1):224–9, 1999.

[33] Rafael Yuste and Winifried Denk. Dendritic spines as functional units of neuronal integration. *Nature*, 375:682–684, 1995.